Nanoscale

Accepted Manuscript

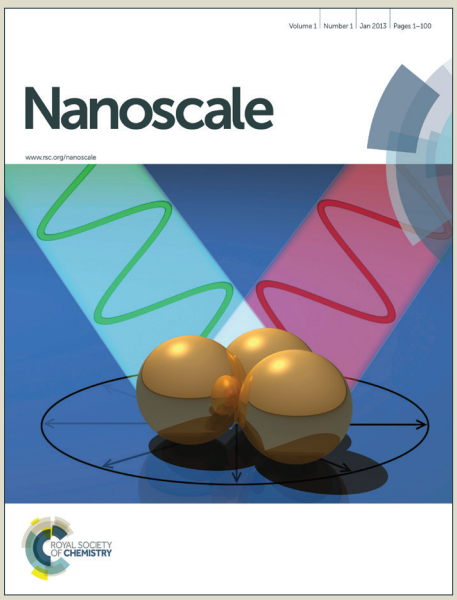

ROYAL SOCIETY OF CHEMISTRY

www.rsc.org/nanoscale

Journal Name

RSCPublishing

ARTICLE

Effect of TiO_2 microbead pore size on the performance of DSSCs with cobalt based electrolyte

Cite this: DOI: 10.1039/x0xx00000x

Yang Chen,[a] Fuzhi Huang,*[a] Wanchun Xiang,[b] Dehong Chen,[c] Lu Cao,[c] Leone Spiccia,[b] Rachel A. Caruso*[cd] and Yi-Bing Cheng*[a]

Received 00th January 2012,
Accepted 00th January 2012

DOI: 10.1039/x0xx00000x

www.rsc.org/

Mesoporous TiO_2 microbeads with well-defined intra-bead pore sizes (14 nm, 23 nm or 33 nm) were employed to investigate the effect of pore size on the performance of dye-sensitized solar cells constructed with an organic dyes (MK2) and a $[Co(bpy)_3]^{2+/3+}$ (bpy = 2,2'-bipyridine) based electrolyte. The $TiCl_4$ post treatment and film thickness were optimized for the TiO_2 electrodes made from beads with 33 nm intra-bead pores, and an overall energy conversion efficiency of 8.5% was achieved for the device with a 6.5 μm thick TiO_2 film treated with a 20 mM $TiCl_4$ solution. Although beads with larger pores had a smaller specific surface area, devices derived from these beads produced better photovoltaic performance. This is attributed to the improved diffusion of cobalt species inside the working electrode, as evidenced by a higher electron lifetime and dye regeneration rate recorded on these solar cells.

Introduction

Dye-sensitized solar cells (DSSCs) have attracted research worldwide because of their low cost, flexibility and colourful characteristics.[1-5] As one of the most important components in a DSSC system, the electrolyte regenerates the oxidized dye molecules, following photon-induced electron injection into the semiconductor, and completes the internal electrochemical circuit between the photoanode and the counter cathode. In the past, the most commonly used electrolyte was based on the I^-/I_3^- redox couple, which has achieved an efficiency of 11.5 % under 1 sun illumination.[6] However, there are some drawbacks for such an electrolyte system.[7] The main one is the large mismatch between the oxidation potential and the HOMO level of dye molecules. As a result, the open circuit voltage of DSSCs is limited since it is determined by the difference between the quasi-Fermi level of the TiO_2 semiconductor and the Nernst potential of the redox couple.[8] In addition, a significant portion of the visible light can be absorbed by a high concentration of I_3^- species in the electrolyte, which limits the achievable short circuit photocurrent density (J_{sc}). Moreover, due to corrosion of the I^-/I_3^- redox couple, the long-term stability is greatly impaired.

Among many alternative redox couples, cobalt complexes are attractive alternatives to the traditional I^-/I_3^- redox shuttle because they have low visible light absorption higher redox potential, and are less corrosive. High efficiency above 12% has been reported by using the cobalt electrolyte.[9, 10] The cobalt electrolyte also is compatible to the aqueous solution.[11] However, due to the larger molecular size and mass, in comparison to I^-/I_3^-, cobalt complexes suffer a major limitation as a redox couple due to slow mass transport in the mesoporous TiO_2 photoanode.[7] Indeed, the porosity and the thickness of TiO_2 films were found to be crucial to the performance of DSSCs based on cobalt electrolytes. Yella *et al.* increased the pore size of the photoanode from 23 nm to 32 nm and achieved an unprecedented 12.3% efficiency with cobalt-complexes as the electrolyte.[9] Kim *et al.* increased the TiO_2 film porosity from 0.52 to 0.59 by modifying the ratio of ethyl cellulose (binder) to TiO_2 in the paste, and found improved photovoltaic performance of DSSCs with a cobalt based electrolyte.[12] Tsao *et al.* reported the impact of the $TiCl_4$ post-treatment on TiO_2 film morphology and the diffusion of the cobalt based electrolyte.[13] Since the pore size is very important for cobalt system, it is necessary to investigate the pore size effect to find the optimized pore size. However, as the traditional nanocrystalline TiO_2 films have a wide pore size distribution, it is unlikely to determine the optimized pore size.

In this paper, 830 ± 40 nm sized TiO_2 beads with 14, 23 or 33 nm mesopores, denoted as B14, B23 and B33, were employed to study the effect of pore size on the performance of cobalt electrolyte based DSSCs. Different from typical TiO_2 nanocrystals, mesoporous TiO_2 microbeads can be fabricated with well-controlled diameter and defined pore sizes,[14] thus they are ideal for investigating the effect of pore size on the diffusion of cobalt-complexes as the redox couple and the photovoltaic performance of DSSCs. In addition, the interconnected large inter-beads pore in the film can provide a fast diffusion channel for the cobalt species.[15, 16] Recently, both Grätzel[15] and Hagfeldt[16] groups have found the large inter-beads pore facilitated the cobalt diffusion and improved the PCE of the cobalt electrolyte based DSSCs.

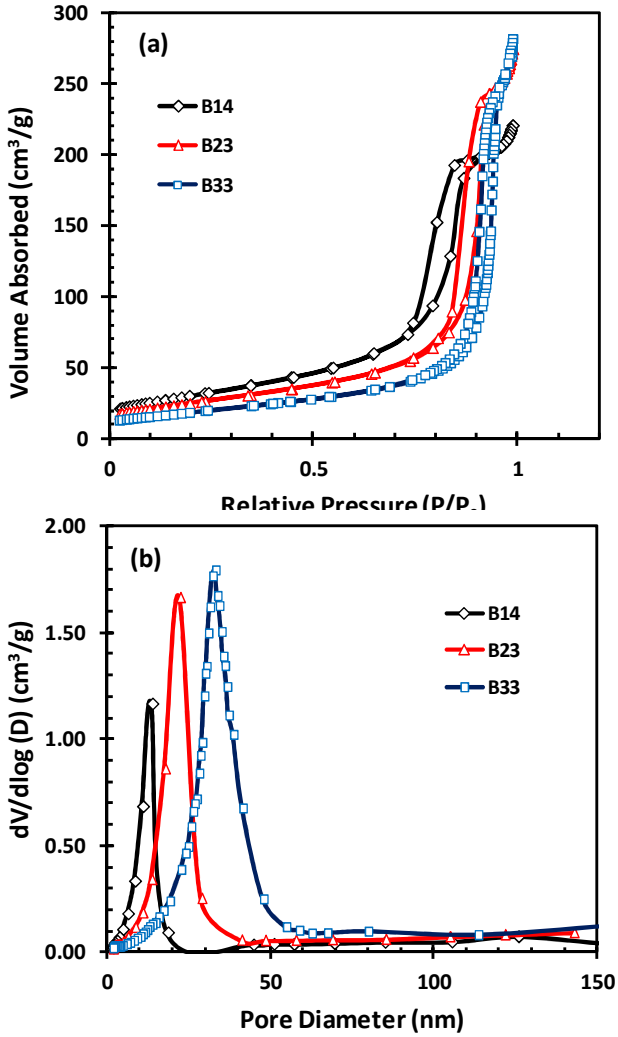

Fig. 1 a) Nitrogen sorption isotherms b) and corresponding pore size distribution of the mesoporous TiO2 beads.

Table 1 Intra-bead pore size and specific surface area of the mesoporous TiO2 beads calculated form nitrogen sorption isotherms, and the estimated inter-bead pore using face-centered cubic close packing model of the identical spheres.

Sample	Intra-bead pore Size (nm)	Inter-bead pore size (nm)	Surface area (m^2/g)
B14	14 ± 1	187 ± 9	108.0 ± 0.7
B23	23 ± 2	187 ± 9	89.1 ± 0.5
B33	33 ± 2	187 ± 9	71.0 ± 0.5

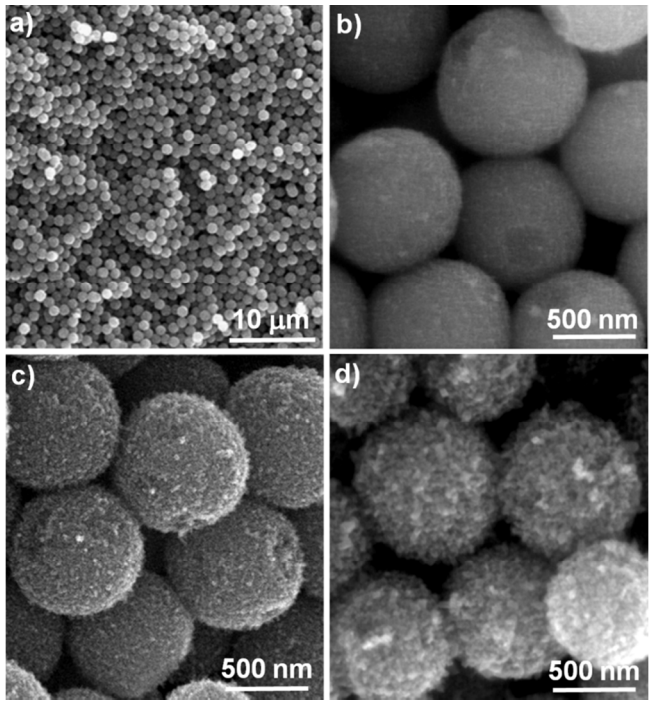

Fig. 2 SEM images of the monodisperse mesoporous TiO_2 beads (830 ± 40 nm) with featuring pore size of 14 ± 1 nm (a, b), 23 ± 2 nm (c), and 33 ± 2 nm (d). Note: all these images were obtained without metal sputter coating of the samples.

Results and discussion

Mesoporous TiO_2 microbeads with variable pore size

Nitrogen gas sorption was used to characterize the pore size distribution and surface area of the synthesized microbeads. Large mesopores were present in the three samples (B14, B23, and B33), confirmed by a sharp capillary condensation step as well as a H1-type hysteresis loop at relative pressures (P/P_0) between 0.82 and 0.96 in the Type IV isotherms (Fig. 1 a). As shown in Fig. 1 b), all samples show a narrow pore size distribution, indicating a well-controlled pore size in these materials. The pore size and surface area calculated from the gas sorption data (Table 1) indicate that as the pore size of the beads increases from 14 nm to 33 nm, there is a gradual decrease in surface area from 108.0 m^2/g to 71.0 m^2/g.

The morphologies of the TiO_2 beads with diverse pore sizes (14 nm, 23 nm and 33 nm) are shown in Fig. 2. All these beads possess a similar diameter of 830 ± 40 nm and are composed by anatase nanocrystals of varied sizes. Among these TiO_2 beads, a comparatively rougher surface was observed for the 33 nm pore sized beads, indicating a larger crystal size for this sample.

As shown in the cross section images (Fig. 3), there are two types of pores in the mesoporous TiO_2 bead film. The inter-bead pores between TiO_2 beads, the size of which estimated based on face-centered cubic close packing is around 187 nm, and the mesopores that exist within the TiO_2 beads. Thus, the mesoporous TiO_2 microbeads can be synthesized with a well defined and controllable intra-bead pore size (14, 23 or 33 nm), which is ideal for investigating the effect of pore size on the diffusion properties of the cobalt electrolyte. As seen in Fig. 3, after a full sintering, the connections between TiO_2 beads are improved, but the inter-bead pore size is still very large. As the size of cobalt based redox couples is around 1-2 nm,[17] there should be no difficulty for mass diffusion within the large inter-bead pores. However, diffusion of the cobalt complex may be hindered within the small intra-bead mesopores.

Optimization of working electrodes

A $TiCl_4$ post treatment is often used on nanocrystalline TiO_2 films for DSSCs using the I^-/I_3^- electrolyte to improve the J_{sc} and fill factor.[18] $TiCl_4$ treatment was also found to suppress the electron/electrolyte recombination in TiO_2 films.[18-22] However,

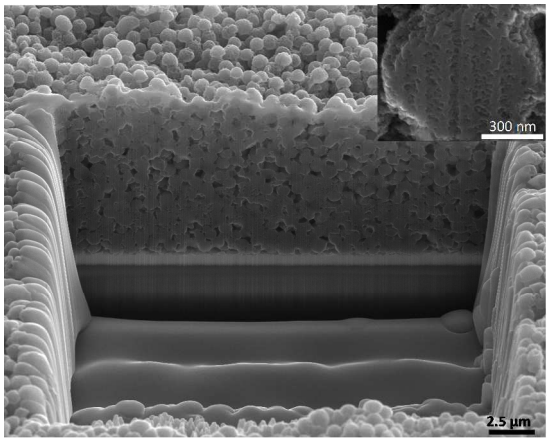

Fig. 3 Cross section SEM image of a bead electrode composed of B23 beads. Inset – cross section SEM image of a single B23 bead. The cross sections were produced by focused ion beam (FIB) milling.

Table 2 Photovoltaic parameters of the DSSCs employing bead electrodes treated with TiCl4 of three different concentrations (10, 20 and 40 mM).

Sample	V_{oc} (mV)	J_{sc} (mA/cm^2)	*FF*	*PCE* (%)
B23-10 mM	914 ± 2	8.4 ± 0.1	0.74 ± 0.01	5.7 ± 0.1
B23-20 mM	913 ± 3	10.1 ± 0.1	0.79 ± 0.01	7.3 ± 0.1
B23-40 mM	882 ± 2	4.7 ± 0.1	0.77 ± 0.01	3.2 ± 0.1

V_{oc} is open circuit photovoltage, J_{sc} is the short circuit photocurrent, *FF* is the fill factor, and *PCE* is the power conversion efficiency.

both the pore size and porosity of the TiO_2 films can be affected by the concentration of the $TiCl_4$ solution used in post treatment,[20, 21] and these parameters can influence the photovoltaic performance of the DSSCs utilizing cobalt electrolytes.[13] Therefore, it is necessary to optimize the $TiCl_4$ concentration for the post-treatment of TiO_2 working electrodes. Electrodes made from TiO_2 beads with 23 nm mesopores were treated with three different $TiCl_4$ concentrations, 10, 20 and 40 mM, for this purpose. According to the photovoltaic results (Table 2), the 20 mM $TiCl_4$ treated electrode yields the highest energy conversion efficiency, mainly because of the high photocurrent generated. The result highlights that the 40 mM $TiCl_4$ post-treatment commonly used for DSSCs with the iodine/iodide electrolyte is not optimal for DSSCs assembled with electrodes composed of microbeads and the cobalt electrolyte, as a low photocurrent of 4.7 mA/cm^2 was obtained. Both mesopore size and porosity would be expected to decrease with increasing $TiCl_4$ concentrations due to the thicker TiO_2 coating. Hence, mass diffusion of the large cobalt complex is hindered, as further confirmed by the photocurrent transient measurements (See Fig. S1. ESI), which is consistent with the result reported in literature.[13] There is no significant mass transport problem for devices made with the 10 and 20 mM $TiCl_4$ treated electrodes, with the latter resulting in the best performance.

Thickness of the TiO_2 films also plays a vital role as it affects the dye loading and the transport of cobalt complexes within the film and, thus, the overall photovoltaic performance. It also affects recombination events occurring at the TiO_2/electrolyte interface, as the recombination probability increases with film thickness. Therefore, it is necessary to optimize the film thickness before investigating the effect of the mesopore size of

Table 3 Photovoltaic properties of the DSSCs employing bead electrodes of varied thicknesses and cobalt electrolyte at different light intensities.

Sample	Light intensity (mW/cm^2)	V_{oc} (mV)	J_{sc} (mA/cm^2)	*FF*	*PCE* (%)
B33-3.5 µm	10	836 ± 2	0.9 ± 0.1	0.82 ± 0.01	6.6 ± 0.1
	100	897 ± 3	10.0 ± 0.1	0.79 ± 0.01	6.5 ± 0.1
B33-6.5 µm	10	786 ± 2	1.3 ± 0.1	0.78 ± 0.01	8.1 ± 0.1
	100	858 ± 1	12.7 ± 0.1	0.77 ± 0.01	8.5 ± 0.1
B33-9.5 µm	10	824 ± 2	1.4 ± 0.1	0.78 ± 0.01	9.0 ± 0.1
	100	877 ± 2	10.3 ± 0.1	0.72 ± 0.01	6.5 ± 0.1

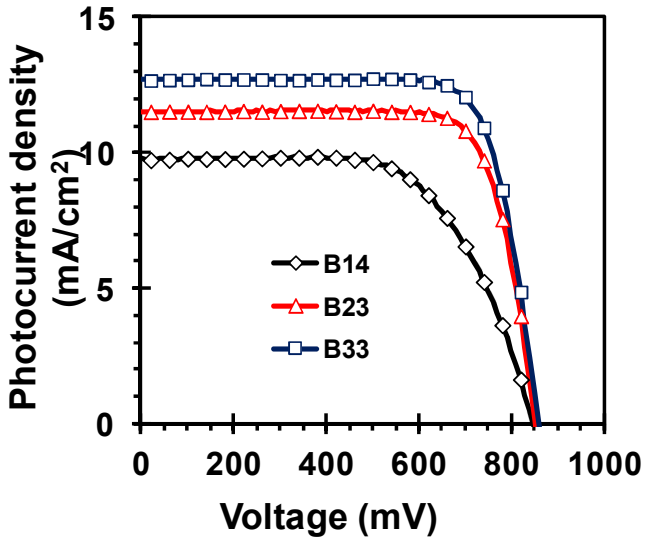

Fig. 4 J-V curves of the DSSCs constructed using B14, B23, and B33 bead electrodes with a film thickness of 6.5µm.

beads on the performance of DSSCs made using cobalt electrolytes. The effect of TiO_2 film thickness on photovoltaic properties was characterized by using 33nm pore-sized beads (B33) with three different film thicknesses (3.5, 6.5 and 9.5 µm). Since an organic sensitizer MK2 with high extinction coefficient was used, the relatively thinner TiO_2 photoanodes can be employed to construct high efficiency solar cells. These electrodes were treated with 20 mM $TiCl_4$. Table 3 summarises the resulting photovoltaic properties of films with different thickness. It is notable that when the thickness of TiO_2 films increased from 3.5 to 6.5 µm, the photocurrent increased by 2.7 mA/cm^2 and the conversion efficiency increased by 2 % at 1 sun illumination. This is attributed to the increased dye uptake in the thicker TiO_2 film. However, when further increasing the film thickness to 9.5 µm, the J_{sc} at 1 sun illumination significantly dropped to 10.3 mA/cm^2. This drop in J_{sc} can be related to slower (or restricted) transport of the large cobalt complexes in the electrolyte, as reflected by the non-linear increase in the photocurrent density with incident light intensity, viz, the photocurrent under 100 % illumination is not 10 times that under 10 % illumination. As shown in Table 3, at 10 mW/cm^2 the J_{sc} measured from the 9.5 µm film device is 1.4 mA/cm^2 and hence the J_{sc} was expected to be around 14 mA/cm^2 at 100 mW/cm^2 illumination. For the thinner TiO_2 films of 3.5 µm and 6.5 µm thickness, the photocurrent

Table 4 Photovoltaic performance of the DSSCs constructed using B14, B23, and B33 bead electrodes with a film thickness of 6.5µm.

Sample	V_{oc} (mV)	J_{sc} (mA/cm^2)	*FF*	*PCE* (%)
B14	847 ± 2	9.8 ± 0.1	0.64 ± 0.01	5.3 ± 0.1
B23	849 ± 1	12.2 ± 0.1	0.71 ± 0.01	7.3 ± 0.1
B33	858 ± 3	12.7 ± 0.1	0.77 ± 0.01	8.5 ± 0.1

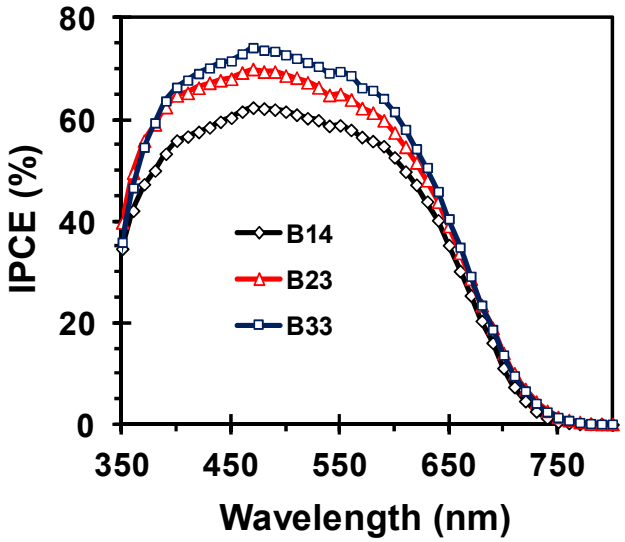

Fig. 5 Incident photon-to-current conversion efficiencies (IPCEs) spectra of the DSSCs constructed using B14, B23, and B33 bead electrodes with a film thickness of 6.5µm.

densities show an almost linear increase with incident light intensity.

In summary, optimization of the $TiCl_4$ post-treatment and film thickness for the TiO_2-bead-based DSSCs assembled with the cobalt electrolyte resulted in a best device performance of 8.5% for a 6.5 µm film post-treated with a 20 mM $TiCl_4$ solution.

Effect of TiO_2 bead pore size on the performance of DSSC devices

To investigate the effect of pore size on the diffusion of cobalt-complex redox species and the photovoltaic performance of DSSCs, 830 ± 40 nm sized TiO_2 beads with 14, 23 and 33 nm mesopores were employed to fabricate the photoanode. Determination of the dye loading by UV/Vis absorbance measurements (Fig. S2) revealed that B14 had the highest dye loading, followed by B23 and B33. This is consistent with the specific surface area of each material which was highest for B14 (108.0 m^2/g, see Table 1).

The photocurrent-voltage curves of DSSCs constructed with the different beads are shown in Fig. 4 and the detailed parameters are listed in Table 4. The best energy conversion efficiency of 8.5 % under 1 sun illumination is achieved on the solar cells constructed using B33 sample with a higher short-circuit photocurrent density (J_{sc}), open circuit voltage (V_{oc}), and fill factor (*FF*). Incident photon-to-current efficiency (IPCE) measurements were performed for DSSCs constructed with different pore sized beads, and the resulting IPCE plots are displayed in Fig. 5. The devices exhibit good light harvesting in the wavelength range of 400-600 nm. The IPCE improved with

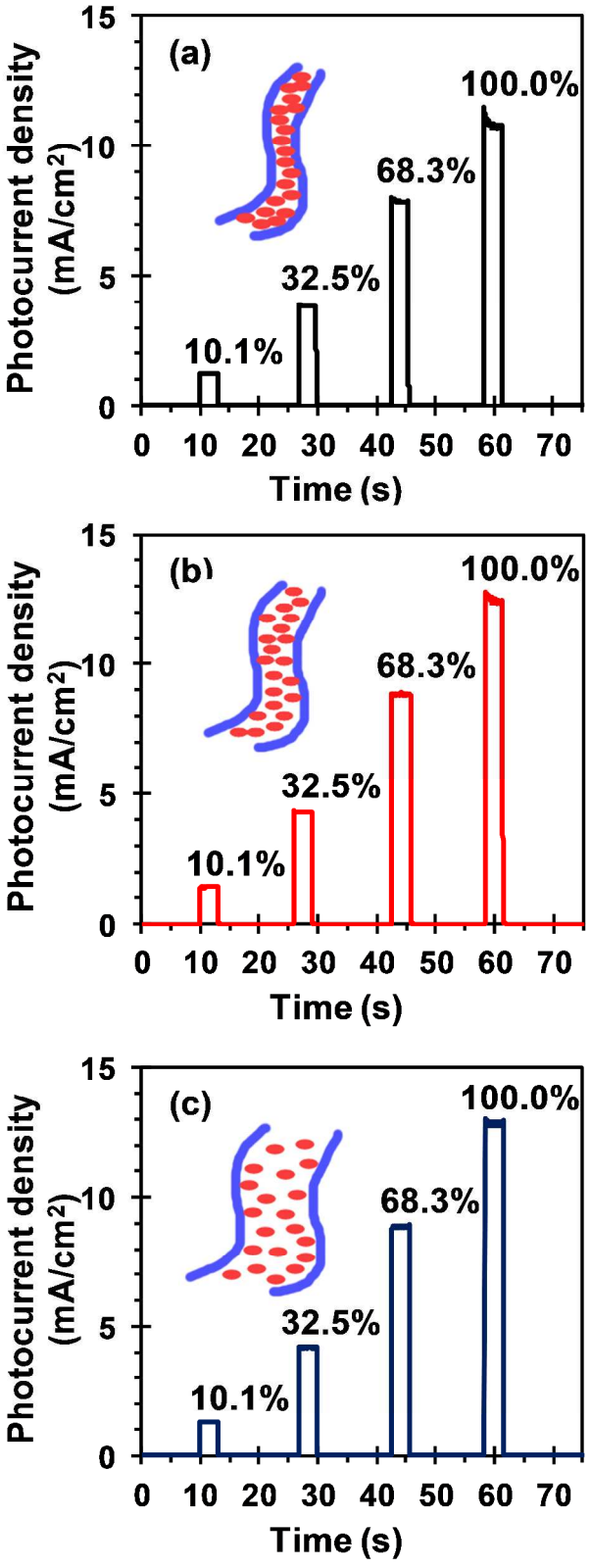

Fig. 6 Photocurrent transient plots measured under illumination intensities of 10.1, 32.5, 68.3 and 100 mW/cm^2 for DSSCs constructed using (a) B14, (b) B23, and (c) B33 bead electrodes with a film thickness of 6.5µm. Insets are illustrations indicating the difference in size between the cobalt redox complexes (red dots) and the width of the mesopores (blue) within the TiO_2 beads.

the increase in bead pore size from 14 to 33 nm, which corresponds to the photovoltaic properties listed in Table 4. The maximum IPCE for DSSCs employing B33 beads is 74.5 %, whereas those for DSSCs with B23 and B14 are 70.3 % and 63.8 %, respectively. It is notable that the J_{sc} of the device with B33 is the highest, even though B33 beads have a relatively low specific surface area (Table 1) and electrodes with such beads have a lower dye loading (ESI Fig. S2). In contrast, the B14 bead electrodes with the highest specific surface area and dye loading amount generated the lowest J_{sc} of 9.8 mA/cm^2. Similar trends could be observed for the V_{oc} and fill factor of these devices. The observed IPCE enhancement for the DSSC derived from B33 beads is probably due to the better diffusion of large cobalt species, which is further supported by the following photocurrent transient and electron lifetime analysis.

To probe the transport of the cobalt electrolyte within the working electrodes, photocurrent transient measurements were conducted under four different illumination conditions, namely light intensities of 10.1, 32.5, 68.3 and 100.0 %. In a typical transient spectrum, a maximum photocurrent (J_{max}) could be observed at the beginning of illumination. The initial maximum photocurrent density is a result of a uniform distribution of cobalt species over the mesoporous TiO_2 film, providing a sufficient concentration of Co^{2+} species to regenerate oxidized dye molecules. Under low light intensity, the amount of photo-excitation in a device is relatively low and the electrochemical reaction between the oxidised dye and cobalt redox mediator remains at equilibrium a stable saturated photocurrent (J_{sat}) is maintained with time. When the light intensity increased, a decay in the photocurrent with time can be seen because the slow transport of cobalt species to and from the film surface causes a decrease in the concentration of Co^{2+} near the TiO_2 surface, thus impairing dye regeneration and photocurrent density. The difference between the initial maximum photocurrent and saturated photocurrent, ΔJ_{sc}, correlates to the dye regeneration efficiency, which can be calculated by the following equation:[12]

$$Regeneration\ efficiency = J_{sat}/J_{max} \times 100\% \quad (1)$$

As seen in Fig. 6, DSSCs constructed with the mesoporous TiO_2 beads of different mesopore sizes exhibit different photocurrent transient behavior. It is clear that the devices made from B33 beads exhibit almost no difference between J_{max} and J_{sat}, whereas for DSSCs with B23 beads a small ΔJ_{sc} (0.10 mA) is observed under 100 % illumination (1 sun condition) but the difference diminishes under lower light intensities. However, for DSSCs with the B14 beads, there is a large ΔJ_{sc} (0.73 mA/cm^2) under 100 % illumination (and also even under 68.3% illumination), indicating significant diffusion problems in such a bead electrode. The calculated dye regeneration efficiencies (Table S1) indicate the underlying cobalt diffusion problem, which causes a decrease in the photocurrent densities of DSSCs constructed using B23 and B14 beads (Fig. 6).

The fast diffusion of the Co-based redox couple in the DSSC made from 33nm pore-sized beads (B33) is also reflected in the fill factor, as this is influenced by the internal resistance. The open circuit photovoltage is normally affected by the charge recombination at the interface of TiO_2 and the redox couple.[23] The device derived from B33 beads achieved a relatively higher V_{oc} (858 mV), indicating less charge recombination occurred at the TiO_2/electrolyte interface, which is confirmed by the electron lifetime results calculated from the intensity modulated photovoltage spectroscopy (IMVS) measurements (Fig. 7).

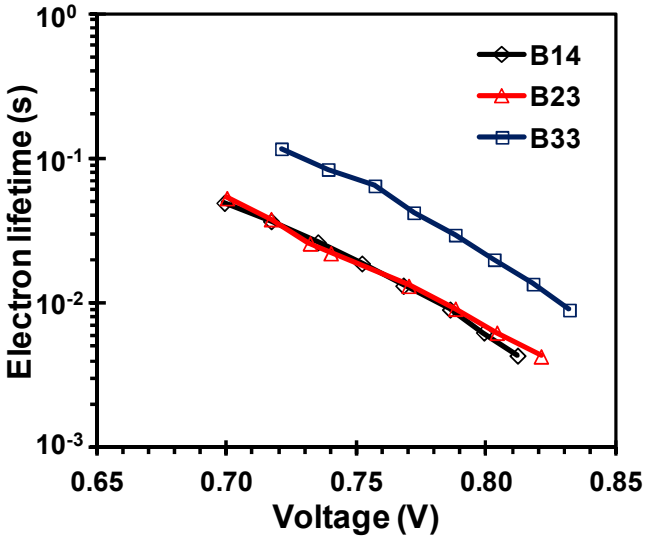

Fig. 7 Electron lifetimes of the DSSCs constructed with B14, B23, and B33 bead electrodes with a film thickness of 6.5μm.

The recombination kinetics were investigated using IMVS to probe the effects of mesopore sizes on the electron lifetime. Electron lifetime (τ_n) can be obtained from the frequency (f_{min}) at the top of the semicircle in the Nyquist plots or the peak frequency in the Bode plots by the equation $\tau_n = (2\pi f_{min})^{-1}$.[24] The DSSC constructed with B33 beads exhibits a higher electron lifetime in comparison with those made with the B23 and B14 beads, Fig. 7. The improvement in the lifetime at similar open circuit voltage highlights the fact that the recombination under illumination is dramatically slower when employing B33 beads. As discussed above, the diffusion of cobalt species is a serious problem for electrodes with small pore-sized beads, and this impairs dye regeneration. As a result of the slow transport of cobalt species near TiO_2 surface there is an increase in the probability of recombination between injected electrons in the conduction band of TiO_2 and Co^{3+} species in the electrolyte. The large inter-bead pores do not act as a barrier for diffusion of the cobalt complex, the bottleneck is the intra-bead mesopores present in individual microbeads. Obviously, TiO_2 microbeads with large internal mesopores have great advantages for DSSCs employing the cobalt electrolytes.

Conclusion

Mesoporous TiO_2 microbeads with tunable pore sizes of 14, 23 or 33 nm were synthesized to investigate the effect of mesopore size on the diffusion of the cobalt-complex redox couple and the photovoltaic performance of the DSSCs. To optimize the cell performance a bead film thickness of 6.5 μm and a $TiCl_4$ post treatment concentration of 20 mM were determined. It was found that small pore (14 nm) would induce the cobalt electrolyte diffusion problem and result in a low photocurrent. Mass transport of the cobalt redox electrolyte within the electrodes was significantly improved when employing the large (33 nm) pore-sized TiO_2 beads (B33), giving a remarkable overall conversion efficiency of 8.5 %.

Experimental Section

Materials and reagents

All chemicals were used as received. The water used in all experiments was produced in a Millipore Milli-Q purification system and had a resistivity higher than 18.2 MΩ cm. The organic solvents used for reactions were obtained from Merck Specialty Chemicals (Sydney, Australia). All the other chemicals were purchased from Sigma-Aldrich.

Cobalt complex and electrolyte preparation

The tris(2,2'-bipyridine) cobalt(II) / (III) bis(trifluoromethane) sulfonimide complexes ($[Co(bpy)_3]$ $(TFSI)_2$) and $[Co(bpy)_3]$ $(TFSI)_3$ were synthesized according to the literature.[25] Briefly, one equivalent of $CoCl_2.6H_2O$ and 3.3 equivalents of 2,2'-bipyridine were dissolved in a minimal amount of methanol, and the solution was stirred at reflux for 1 h. An excess of lithium bis(trifluoromethane-sulfonyl)imide (LiTFSI) was then added to the solution to precipitate the cobalt complex. The solid was filtered, washed with diethyl ether and dried under vacuum for 24 h. Oxidation of the Co^{II} complex was achieved by adding slightly more than one molar equivalent of $NOBF_4$ to an acetonitrile solution of the complex. The solvent was removed by rotary evaporation. The complex was redissolved in acetonitrile and a 10 fold excess of LiTFSI was added to precipitate the product that was then filtered, washed with diethyl ether and dried at 70 ºC under vacuum for 24 h. These two compounds were used without further purification. The cobalt electrolyte was then prepared from these complexes and consisted of 0.2 M $[Co(bpy)_3](TFSI)_2$, 0.07 M $[Co(bpy)_3]$ $(TFSI)_3$, 1.0 M 4-*tert*-butylpyridine (TBP) and 0.05 M lithium bis(trifluoromethane)sulfonamide in acetonitrile.

Titania bead synthesis

The mesoporous TiO_2 microbeads with well-controlled diameters and pore sizes were synthesized by a combined sol-gel and solvothermal process.[14] The mesopores sizes between the anatase nanoparticles within the beads were enlarged by increasing the ammonia concentration during the solvothermal process.[14, 26] The TiO_2 paste was prepared by dispersing the TiO_2 power (5.0 g) in ethanol (45.0 g) followed by sonication for 30 min. Ethyl cellulose (2.5 g) and terpinol (20.0 g) were then added to the suspension, stirring for 30 min. The more volatile ethanol solvent was removed by rotary evaporation at 40 °C for 30 min, leaving a viscous paste that was used to screen-print the TiO_2 microbead films.

Solar cell assembly

A compact blocking layer of TiO_2 was prepared on FTO glass (Nippon, 10 Ω/□) by spray pyrolysis of a 7.5% w/w solution of titanium isopropoxide bisacetylacetonate in ethanol at 450 °C. The TiO_2 bead pastes were then printed onto the FTO glass by using a screen printer. These TiO_2 working electrodes underwent a sintering process in air as follows: 150 °C for 10 min, 325 °C for 5 min, 375 °C for 5 min, 450 °C for 30 min, and 500 °C for 15 min. A metal free dye with high extinction coefficient was used, 2-cyano-3-[5‴-(9-ethyl-9*H*-carbazol-3-yl)-3′, 3″, 3‴, 4-tetra-*n*-hexyl-[2, 2′, 5′, 2″, 5″, 2‴]-quater thiophen-5-yl] acrylic acid, known as MK2, in a 0.2 mM 1:1:1 mixture acetonitrile, tertiary-butanol and toluene solution. The sintered TiO_2 working electrodes were sensitized in the MK2 dye solution overnight and then rinsed with acetonitrile before DSSC construction. Counter electrodes were prepared by thermally decomposing H_2PtCl_6 (10 mM in ethanol) on FTO glass at 400 °C for 15 min. The sensitized working electrode and Pt-coated counter electrode were sealed by a laser engraved 25 μm Surlyn gasket under heat and pressure. The electrolyte was back injected into the assembled DSSCs by using a vacuum chamber. Before soldering on wires, the hole on the counter electrode was sealed by a Surlyn attached aluminium film under heat and pressure.

Characterization

The cross-section morphologies of the beads were examined by a Focussed Ion Beam Scanning Electron Microscope (FEI Quanta 3D FEG). Nitrogen sorption isotherms were conducted by using a Micromeritics Tristar 3000 instrument. The beads were degassed at 160 °C for 18 h and the standard multipoint Brunauer-Emmett-Teller (BET) method was employed to calculate the specific surface area. The pore size distributions were derived based on the Barrett-Joyner-Halenda (BJH) model.

A black metal mask with aperture size of 0.36 cm^2 was employed to shield the constructed solar cells. Current-voltage (I-V) curves for the solar cells were obtained by using a Keithley 2400 source meter under simulated illumination of a xenon lamp (Oriel) fitted with an AM1.5 filter. Incident photon-to-current conversion efficiency (IPCE) plots as a function of excitation wavelength were obtained by using a Keithley 2400 source meter under the irradiation of a 300 W xenon lamp equipped with an Oriel Cornerstone 260 ¼ m monochromator.

Dye desorption measurements were carried out by detaching the dye from the photoanodes using a 0.01 M KOH in 1:1:1 (by volume) solution of acetonitrile, tert-butanol and toluene. UV-Vis absorbance measurements were then conducted on these dye containing KOH solutions using a CARY50 Bio UV-Vis spectrophotometer.

Intensity-modulated photovoltage spectroscopy (IMVS) experiments were carried out using a Zahner CIMPS/CIMVS system. Illumination was provided by a 670 nm light emitting diode. The amplitude of the sinusoidal modulation for IMVS measurements was less than 5% in the frequency range of 10^{-2} - 10^5 Hz. Zview software was then used to get the peak frequency by curve fitting the resulting plot.

Transient photocurrent measurements were carried out on a BioLogic VSP electrochemical workstation, and the cell was illuminated using the solar simulator. The light source was switched on and off and the photocurrent was recorded by the electrochemical workstation using a chronoamperometry (CA) technique in the EC-Lab software (Bio-Logic Science Instruments).

Acknowledgements

The Australian Research Council is acknowledged for support through the Discovery Project Scheme (DP110101346) and a Future Fellowship for R. A. C. (FT0990583). Facilities supported by the Victorian Organic Solar Cells Consortium were used for this study. YC is a recipient of a Monash University postgraduate scholarship.

Notes and references

[a] Department of Materials Engineering, Monash University, Melbourne, Victoria, 3800, Australia. E-mail: fuzhi.huang@monash.edu; yibing.cheng@monash.edu; Fax: +61 3 9905 4940; Tel: +61 3 9905 4930.
[b] School of Chemistry, Monash University, Victoria 3800, Australia.

[c] PFPC, School of Chemistry, The University of Melbourne, Melbourne, Victoria, 3010, Australia. Email: rcaruso@unimelb.edu.au; Fax: +61 3 9347 5180; Tel: +61 3 8344 7146.
[d] CSIRO, Materials Science and Engineering, Private Bag 33, Clayton South, Victoria, 3169, Australia.

† Electronic Supplementary Information (ESI) available: Photocurrent transient plots of the devices treated with different concentrations of $TiCl_4$ and UV-vis spectra of dye desorption. See DOI: 10.1039/b000000x/

References

1. M. Grätzel, *Nature*, 2001, **414**, 338-344.
2. A. Hagfeldt, G. Boschloo, L. Sun, L. Kloo and H. Pettersson, *Chem. Rev.*, 2010, **110**, 6595-6663.
3. J. Halme, P. Vahermaa, K. Miettunen and P. Lund, *Adv. Mater.*, 2010, **22**, E210-E234.
4. M. Grätzel, *J. Photochem. Photobiol. A: Chem.*, 2004, **164**, 3-14.
5. B. O'Regan and M. Grätzel, *Nature*, 1991, **353**, 737-740.
6. C. Y. Chen, M. K. Wang, J. Y. Li, N. Pootrakulchote, L. Alibabaei, C. H. Ngoc-le, J. D. Decoppet, J. H. Tsai, C. Grätzel, C. G. Wu, S. M. Zakeeruddin and M. Grätzel, *ACS Nano*, 2009, **3**, 3103-3109.
7. H. N. Tian and L. C. Sun, *J. Mater. Chem.*, 2011, **21**, 10592-10601.
8. G. Boschloo and A. Hagfeldt, *Acc. Chem. Res.*, 2009, **42**, 1819-1826.
9. A. Yella, H. W. Lee, H. N. Tsao, C. Y. Yi, A. K. Chandiran, M. K. Nazeeruddin, E. W. G. Diau, C. Y. Yeh, S. M. Zakeeruddin and M. Grätzel, *Science*, 2011, **334**, 629-634.
10. S. Mathew, A. Yella, P. Gao, R. Humphry-Baker, F. E. CurchodBasile, N. Ashari-Astani, I. Tavernelli, U. Rothlisberger, K. NazeeruddinMd and M. Grätzel, *Nat. Chem.*, 2014, **6**, 242-247.
11. W. Xiang, F. Huang, Y.-B. Cheng, U. Bach and L. Spiccia, *Energy Environ. Sci.*, 2013, **6**, 121-127.
12. H.-S. Kim, S.-B. Ko, I.-H. Jang and N.-G. Park, *Chem. Commun.*, 2011, **47**, 12637-12639.
13. H. N. Tsao, P. Comte, C. Yi and M. Grätzel, *ChemPhysChem*, 2012, **13**, 2976-2981.
14. D. H. Chen, L. Cao, F. Z. Huang, P. Imperia, Y.-B. Cheng and R. A. Caruso, *J. Am. Chem. Soc.*, 2010, **132**, 4438-4444.
15. L.-P. Heiniger, F. Giordano, T. Moehl and M. Grätzel, *Adv. Energy Mater.*, 2014.
16. M. Pazoki, N. Taghavinia, A. Hagfeldt and G. Boschloo, *J. Phys. Chem. C*, 2014, **118**, 16472-16478.
17. W. Liu, W. Xu, J.-L. Lin and H.-Z. Xie, *Acta Crystallographica Section E*, 2008, **64**, m1586.
18. B. C. O'Regan, J. R. Durrant, P. M. Sommeling and N. J. Bakker, *J. Phys. Chem. C*, 2007, **111**, 14001-14010.
19. C. J. Barbé, F. Arendse, P. Comte, M. Jirousek, F. Lenzmann, V. Shklover and M. Grätzel, *J. Am. Ceram. Soc.*, 1997, **80**, 3157-3171.
20. S. Ito, P. Liska, P. Comte, R. L. Charvet, P. Péchy, U. Bach, L. Schmidt-Mende, S. M. Zakeeruddin, A. Kay, M. K. Nazeeruddin and M. Grätzel, *Chem. Commun.*, 2005, 4351-4353.
21. P. M. Sommeling, B. C. O'Regan, R. R. Haswell, H. J. P. Smit, N. J. Bakker, J. J. T. Smits, J. M. Kroon and J. A. M. van Roosmalen, *J. Phys. Chem. B*, 2006, **110**, 19191-19197.
22. L.-Y. Zeng, S.-Y. Dai, K.-J. Wang, X. Pan, C.-W. Shi and L. Guo, *Chin. Phys. Lett.*, 2004, **21**, 1835-1837.
23. M. K. Nazeeruddin, A. Kay, I. Rodicio, R. Humpbry-Baker, E. Müller, P. Liska, N. Vlachopoulos and M. Grätzel, *J. Am. Chem. Soc.*, 1993, **115**, 6382-6390.
24. R. Kern, R. Sastrawan, J. Ferber, R. Stangl and J. Luther, *Electrochim. Acta*, 2002, **47**, 4213-4225.
25. W. Xiang, W. Huang, U. Bach and L. Spiccia, *Chem. Commun.*, 2013, **49**, 8997-8999.
26. D. H. Chen, F. Z. Huang, Y.-B. Cheng and R. A. Caruso, *Adv. Mater.*, 2009, **21**, 2206-2210.